Optical assembling dynamics of individual polymer nanospheres investigated by single-particle fluorescence detection

Chie Hosokawa, Hiroyuki Yoshikawa,* and Hiroshi Masuhara†
Department of Applied Physics and Frontier Research Center, Osaka University, 2-1 Yamadaoka, Suita, Osaka 565-0871, Japan
(Received 6 July 2004; published 22 December 2004)

When a laser beam is focused into colloidal nanoparticle suspensions, a number of nanoparticles can be confined in the focal spot due to an optical gradient force. To reveal the assembling dynamics of polymer nanoparticles, the assembling process was investigated by analyzing the time evolution of the fluorescence intensity of the nanoparticles. In a dilute suspension of 100-nm-sized particles, a stepwise increase of the fluorescence intensity corresponding to a trapped single nanoparticle was observed. Statistical analysis revealed that the initial assembling rate of nanoparticles was proportional to the laser power and concentration of particle suspensions as expected from the diffusion equation. In 40-nm-sized particle suspensions, blinking profiles of fluorescence intensity were obtained, in which 2–3 particles were simultaneously trapped and then escaped from the focal point. It is considered from statistical analyses and two-dimensional Monte Carlo simulations that this assembling phenomenon is attributable to cluster formation assisted by optical trapping.

DOI: 10.1103/PhysRevE.70.061410 PACS number(s): 82.70.Dd, 87.80.Cc, 83.10.Pp, 87.64.−t

I. INTRODUCTION

Since the pioneering work by Ashkin and co-workers [1], the possibility of utilizing the mechanical action of optical fields to trap neutral particles has accelerated a wide range of applications [2]. Optical trapping has been developed to a laser manipulation technique, which enables noncontact and nondestructive manipulation of fine particles in solution [3–5]. Most of these approaches have been concentrated on micrometer-sized objects because of the difficulty in trapping and identifying individual nanometer-sized ones. The smaller the particle size is, the weaker the trapping force is, since the trapping potential depends on the particle size in principle. In recent years, some groups [6–8] including ours have developed the laser manipulation technique to handle nanoparticles and polymer chains in solution. We have demonstrated that single polystyrene and gold nanoparticles in solution can be trapped and fixed onto the substrate with laser manipulation and fabrication techniques [9]. Furthermore, when the diameter of a trapped material is smaller than the size of the beam spot of the trapping laser, a number of particles can be trapped and assembled at the focal spot. This "optical assembly" of microparticles was first studied by Burns *et al.* [10,11], who demonstrated that binding forces between dielectric particles can be induced by intense optical fields. This research has been followed by some studies on various forms of optical assembly. An interesting example was given by Mei *et al.* [12]; they constructed a three-dimensional assembly by the interference field of multiple laser beams. As an another example, Tatarkova *et al.* [13,14] created a one-dimensional optical assembling system of microscopic colloidal particles. On the other hand, we have successfully demonstrated optical assembly of polymers; poly (*N*-isopropylacrylamide) [15], sodium dodecyl sulfate/xylene micelles [16], poly (*N*-vinylcarbazole) [17], and wire-type dendrimers [18]. In all cases, when a single laser beam is focused into these polymer suspensions, a number of polymers can be assembled at the focal spot and finally an association of polymers can be formed at the same point. However, it is difficult to reveal the assembling process of the polymers, since polymer-polymer interactions such as the van der Waals attraction, hydrogen bonding network, and physical entanglement of polymer chains are complicated.

This optical assembly recalls the initial stage of aggregation and crystallization of macromolecules, which are subjects of great current interest. The structure of a molecular assembly with a sufficiently measurable size can be determined by x-ray crystallography. However, the growth process, especially the initial stage of association, is beyond our knowledge, since it is difficult to observe it directly. Recently, in order to reveal the growth process of the molecular assembly, the assembling dynamics of colloidal particles has been extensively studied using suspensions of charged and hard spheres [19]. Colloidal particles are easy to handle as good models for molecules, since the particle-particle interaction can be simply described and the size and shape of each particle are almost the same. The recent interest is based on the availability of direct imaging techniques [20,21] using large-sized colloidal particles that allow one to investigate the colloidal dynamics in real space in detail. Theory and computer simulations [22,23] have also been developed to probe their dynamical behavior at the microscopic level.

Even in the case of optical assembly, colloidal suspensions give essential information toward understanding their mechanism and dynamics. In this paper, we investigate the initial optical assembling process of polymer nanoparticles suspended in water. Since the nanoparticles include dyes, fluorescence is detected due to two-photon excitation when they are trapped in the focal spot of an yttrium aluminum garnet (YAG) laser. The time evolution of the fluorescence intensity was analyzed by changing particle sizes, trapping

*Electronic address: yosikawa@ap.eng.osaka-u.ac.jp
†FAX: +81-6-6879-7840. Electronic address: masuhara@ap.eng.osaka-u.ac.jp

laser powers, and concentrations. In contrast to the assembling process of 100-nm-sized particles which were trapped one by one, that of 40-nm-sized particles strongly depended on the laser power. In the case of low laser power (150–450 mW), temporal profiles of fluorescence intensity showed a characteristic blinking, in which 2–3 particles were simultaneously trapped and then escaped from the focal point. From experimental and numerically simulated results, it was revealed that the differences of assembling processes are attributed to the cluster formation assisted by optical trapping.

II. EXPERIMENT

Commercial polystyrene latex particles (Molecular Probes, FluoSpheres carboxylate-modified orange F-8800 and F-8792; diameters 100 and 40 nm) were used as samples. These nanoparticles contain fluorescent dyes which absorb light in the range 500–560 nm with a maximum absorption at 540 nm and fluoresce in the range 550–650 nm with a maximum emission at 560 nm. Samples were diluted to appropriate concentrations with distilled water. It was confirmed by using dynamic light scattering (DLS) (Otsuka Electronics, DLS-70S) that the diameters of the latex particles were 95.3 ± 15 nm for 100-nm-sized particles and 36.3 ± 6 nm for 40-nm-sized particles, and that these particles dispersed well without aggregation. The ratio of isolated and aggregated nanometer-sized particles was investigated by scanning electron microscopy (SEM; DB235, FEI Company). For the SEM observation, the sample (particle concentration 8.8×10^7 particles/ml) was dropped on a glass substrate and dried at room temperature. The zeta potential of the particles was obtained with a zeta potential analyzer (Malvern Instruments, Zetasizer Nano-ZS).

The experimental setup is described in Fig. 1. A 1064 nm fundamental beam from a cw Nd^{3+}:YAG laser (Spectron Laser System, SL-902T 1104) was introduced into an optical microscope (Carl Zeiss, UMSP-50) and focused into a sample with ~ 1 μm spot size with an objective lens ($\times 100$ magnification; numerical aperture 1.25). Sample solutions were dropped in a depression glass slide (1 mm depth) and covered by a cover slip (0.17 mm thickness). Since the dyes included in the nanoparticles absorb the YAG laser light via a two-photon excitation process, fluorescence from nanoparticles captured in the focal spot can be detected without another excitation light source. A focal point was set between 10 and 15 μm from the bottom of the cover slip.

Fluorescence emission collected by the objective passed through a bandpass filter (Melles Griot, FIV-008), and was detected by an avalanche photodiode (APD) (EG&G, SPCM-AQ) in photon counting mode. The average dark count was a few hundred counts/s with an APD. The signal was sampled at 20 Hz using a counter board (Contec, CNT24-4) on a PC.

III. RESULTS

When a 1064 nm cw-laser beam was focused on colloidal nanoparticles, the orange emission of the nanoparticles was observed via an optical microscope due to two-photon excitation. The fluorescence intensity is proportional to the square of the excitation laser power; thus the effective excitation volume is restricted to the central portion of the focal spot, allowing only nanoparticles trapped at the focal spot to be detected as demonstrated in [24]. Therefore, this method is useful for investigation of optical assembling process of nanoparticles.

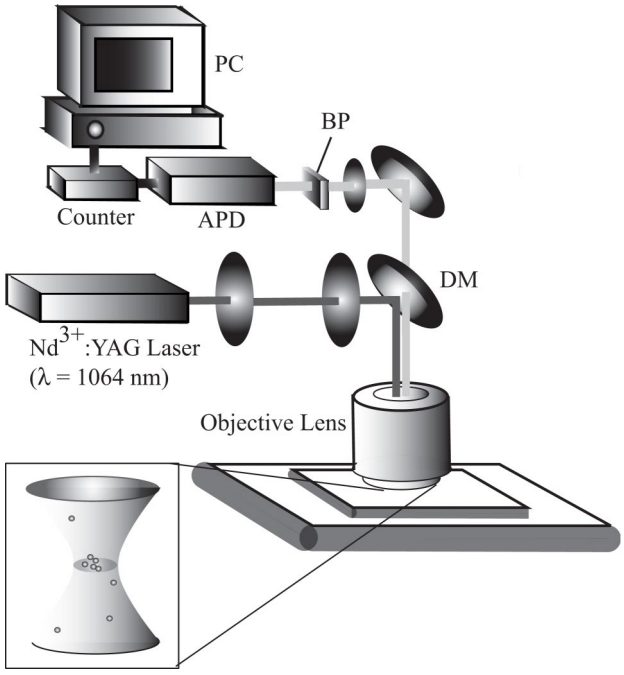

FIG. 1. Schematic diagram of optical setup for optical assembling dynamics studies. A Nd^{3+}:YAG laser beam is focused on the observation plane of the objective. DM, dichroic mirror; BP, bandpass filter; APD, avalanche photodiode; Inset: Schematic illustrations of optical assembling of nanoparticles by optical gradient force.

First, we explain experimental results on 100-nm-sized nanoparticles. Figure 2 shows temporal profiles of fluorescence intensity after laser irradiation in the sample suspension (particle concentration 10^7–10^{12} particles/ml). The increase in fluorescence intensity corresponds to that in the number of trapped nanoparticles. At high concentration, we confirmed that the number of nanoparticles increases continuously with decreasing rate of increment as shown in Fig. 2(a). This shows that nanoparticles are trapped one after another and fill up the focal spot. On the other hand, when the suspension was diluted ($<10^9$ particles/ml), a stepwise increase of fluorescence intensity was observed. A representative temporal profile in a diluted suspension is shown in Fig. 2(b). The mean value of the fluorescence intensity at the first step level was 4893 ± 303 counts/0.05 s. To confirm that the one step is ascribed to a single particle, the fluorescence intensity of a trapped 1-μm-sized particle, which is discerned as a single particle visually under the microscope, was measured using the same microscope. The 1-μm-sized particle, which contains the same concentration of dyes as the 100-nm-sized particle, gave $\sim 4.7 \times 10^6$ counts/0.05 s under the same excitation conditions. Since the ratio of the fluorescence intensity of a 1-μm-sized particle to a 100-nm-sized

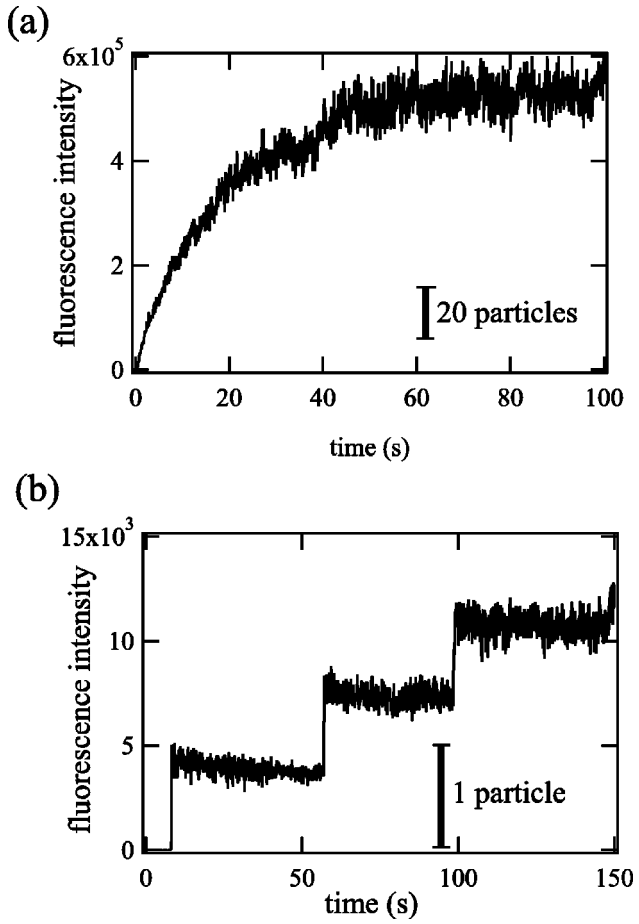

FIG. 2. Temporal trapping profiles of 100-nm-sized particles in water. The photon counts are sampled at each 0.05 s. The concentration of the suspension is (a) 4.3×10^{10} and (b) 4.3×10^{7} particles/ml. Vertical bars indicate fluorescence intensity corresponding to the particle number described beside each bar.

particle should be identical to the volume ratio, the fluorescence intensity of a 100-nm-sized particle is estimated as 4700 counts/0.05 s. This is in good agreement with the experimental results. Consequently, the temporal profile as shown in Fig. 2(b) indicates that 100-nm-sized particles are trapped one by one by an optical gradient force. Apart from the stepwise increase, slight decreases ($\sim$10%/80 s) of fluorescence intensity are observed in individual steps due to photobleaching. Since we use the time and the fluorescence intensity at the moment when the nanoparticles are trapped in the focal spot for the following analysis, photobleaching induced by the trapping laser does not influence it. This assembling process can be described as Brownian motion of individual nanoparticles under the external potential energy $U_{\mathrm{trap}}\cong-\alpha|\mathbf{E}|^2/2$. The trapping potential shape is ascribed to the intensity distribution of the laser beam whose region is experimentally and numerically determined to be ~1 μm in the focal plane and ~3 μm on the optical axis, respectively. When the trapping potential energy is introduced in a diffusion equation, the probability flux [25] per unit area of the nanoparticle suspension, namely, the number of nanoparticles trapped in the focal spot in unit time, is defined as

$$J(r)=-D\left(\frac{\partial C}{\partial r}+\frac{C}{k_BT}\frac{\partial U_{\mathrm{trap}}}{\partial r}\right), \tag{1}$$

where D is the diffusion coefficient, C is the concentration (particles/ml) of the nanoparticle suspension, and r is the distance from the focal point of the laser. Since C is independent of r under the initial conditions, the first term of Eq. (1) can be neglected just after the irradiation. The assembling rate of particles corresponds to the total flux J_{trap}, which is defined as the number of particles passing through a spherical surface around the focal point in unit time,

$$J_{\mathrm{trap}}=-4\pi r^2D\frac{C}{k_BT}\frac{\partial U_{\mathrm{trap}}}{\partial r}. \tag{2}$$

By substituting a Gaussian intensity profile of the trapping laser beam into Eq. (2), the assembling rate J_{trap} can be described as

$$J_{\mathrm{trap}}\propto DC\alpha I_0, \tag{3}$$

where I_0 is the laser power. These equations lose accuracy in a highly concentrated suspension because particle-particle interactions cannot be neglected in the assembling process. For instance, in the case of adsorption and diffusion of micrometer-sized paramagnetic particles in a magnetic potential well, long-range magnetic interparticle interactions must be taken into account [26–28]. In general, however, electrostatic forces between colloidal particles are screened by counterions, so that they are effective at short range as compared to their radii [29]. In the present case, since the early stage of assembling (until a few nanoparticles are trapped) is treated in Eq. (1), particles are separated by large distances and electrostatic interactions can be neglected. Thus single-particle counting in dilute suspension is indispensable to obtain accurate estimations.

We simply demonstrated the validity of the relation (3) by a statistical analysis of our experimental results. Figures 3(a) and 3(b) show the mean values of assembling rates (particles/s) as a function of concentration and laser power, respectively. The assembling rates of nanoparticles were estimated from the reciprocal of the laser irradiation time which is taken until the first particle is trapped. This corresponds to the number of trapped nanoparticles in unit time (particles/s). Figure 3 shows that the assembling rates are proportional to the concentration of nanoparticle suspension and the laser power with slopes of 0.8 and 1.2, respectively, indicating that the assembling process of 100-nm-sized particles is consistent with the relation (3), i.e., it is a diffusion-limited process. It was also confirmed that this relation is applicable for 200-nm-sized particle suspensions.

In contrast to the 100-nm-sized particles, 40-nm-sized particles showed a characteristic assembling process depending on the laser power, as shown in Fig. 4. In the case of 300 mW of laser power, packets of a specified fluorescence intensity (500–1000 counts/0.05 s), were observed in the temporal profile. Since the fluorescence intensity of a single particle was estimated as $\sim$250 counts/0.05 s at the laser power of 300 mW, the temporal profile indicates that 2–3 particles were trapped and escaped simultaneously. Strictly speaking,

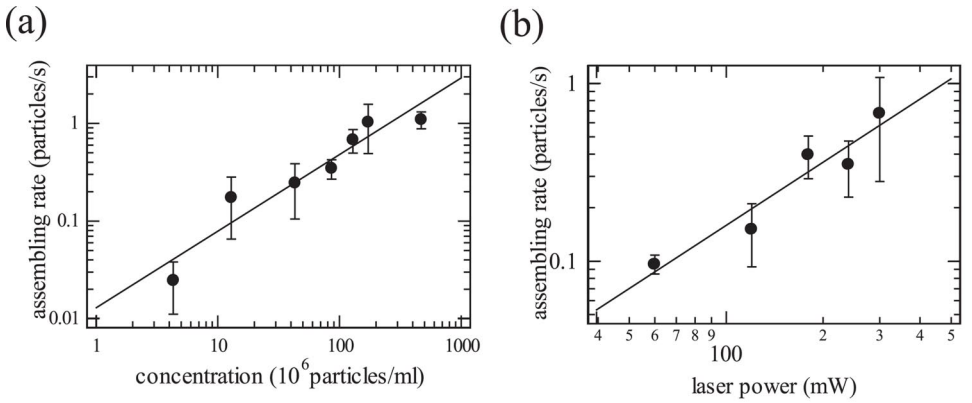

FIG. 3. Assembling rates of 100-nm-sized particle suspensions as functions of concentration and incident laser power. (a) Concentration dependence of the assembling rates at the laser power of 300 mW. (b) Laser power dependence of the assembling rates at the concentration of 1.3×10^8 particles/ml. Solid lines show linear relations.

this is not an assembling process because the trapped nanoparticles escape before the trapping of another nanoparticle. Optical assembling is realized when the trapping rate (number of nanoparticles trapped in unit time) exceeds the escape rate. To achieve it, you have a choice between two methods: one is the increase of laser power and the other is the increase of concentration. However, it is interesting that the methods give different results. At higher laser power (900 mW), it was observed that the number of nanoparticles increased stepwise one by one, as shown in Fig. 4(b), which is a similar profile to that of 100-nm-sized particle suspensions. On the other hand, nanoparticles were assembled with an increasing amount of several particles in a higher-concentration sample, as shown in Fig. 4(c). In the case of 100-nm-sized particles, the laser power I_0 and concentration C contribute to the assembling process in the same way as represented by relation (3), and actually this is demonstrated in Fig. 3. The experimental results of 40-nm-sized particles cannot be represented by a simple diffusion-limited process described as relation (3).

One likely cause for the characteristic assembling of 40-nm-sized particles is aggregation which has occurred before laser irradiation. However, the percentage of aggregates included in the original solution was estimated as 2.5% (i.e., 2.2×10^6 particles/ml) from SEM measurements (3 aggregates/120 particles). This may be an overestimation because the sample prepared for SEM measurement includes aggregates formed during the evaporation of water. When such aggregates (doublets) are suspended in water, from the relation (3), it is expected that the first aggregate would be trapped around 2.2×10^2 s after starting the laser irradiation under the same conditions as in Fig. 4(a). In practice, however, it took only 10.9 s on average. This demonstrates that the event takes place more frequently and the characteristic assembling of 40-nm-sized particles cannot be explained by trapping of aggregates included in the original suspension.

Let us consider the size and laser power dependencies of the assembling processes. In the case of Fig. 4(a), even if 40-nm-sized nanoparticles are once trapped in the focal spot, they escape before the next one is trapped, so that the number of trapped particles does not increase. This is caused by the potential energy of a 40-nm-sized particle whose depth is comparable to the energy of Brownian motion. Actually each depth of the trapping potential ($|U_{\min}| = I_0 \alpha / c n_2 \varepsilon_0$) is $105kT$ for 100-nm-sized particles and $6.7kT$ for 40-nm-sized ones at laser power of 300 mW. That is, if the focused laser beam is introduced into a polydispersed suspension including different sized particles, the escape time, which is determined by the duration of trapping of one particle or aggregate, reflects the particle size [30]. We ascertained that the escape time that was obtained from the temporal profiles [see Fig. 4(a)] correlated with the fluorescence intensity. These results suggest that the unexpected fluorescence signals shown in Fig. 4(a) are attributed to aggregates which were generated during optical trapping.

In other words, clustering took place in advance of assembling in Fig. 4(a), while nanoparticles were assembled one by one in Figs. 2(b) and 4(b). We suppose that this difference originates from the relation between three frequencies of optical trapping, escape, and clustering, which are defined by the number of trapping, escape, and clustering events in unit time. On the basis of this consideration, we propose one model as follows. Nanoparticles form clusters with each other with a certain possibility by getting over the repulsive potential of electric double layers. If the depth of the trapping potential is larger than the kinetic energy of Brownian motion and the repulsive interparticle potential is large enough to prevent clustering for a while, nanoparticles are trapped at the focal spot one by one, because the trapping frequency exceeds the escape frequency and the clustering frequency around the focal spot is low. That is, nanoparticles are captured before cluster formation and this corresponds to assembling of 100-nm-sized particles [see Fig. 2(b)]. On the other hand, when the trapping frequency is comparable to the escaped one and the clustering frequency around the focal spot is high, i.e., when the depth of the trapping potential and repulsive interparticle interaction are small (weak), formed clusters possessing large polarizability are trapped and stay at the focal spot for a relatively long time. From the difference between Figs. 4(a) and 4(b), it is clear that the above two cases are interchanged between two laser powers (300 and 900 mW) in the case of 40-nm-sized particles. In contrast, the more concentrated sample of 40-nm-sized particles gives higher trapping and clustering frequencies, so that aggregates are trapped and fill the focal spot [see Fig. 4(c)].

To evaluate the validity of this model, the assembling process of nanoparticles was investigated by Monte Carlo (MC) simulation, which calculates the Brownian motion of nanoparticles under the optical gradient force in a two-dimensional (2D) system. In 100-nm-sized particle suspensions, the simulated temporal profiles, where the particles are

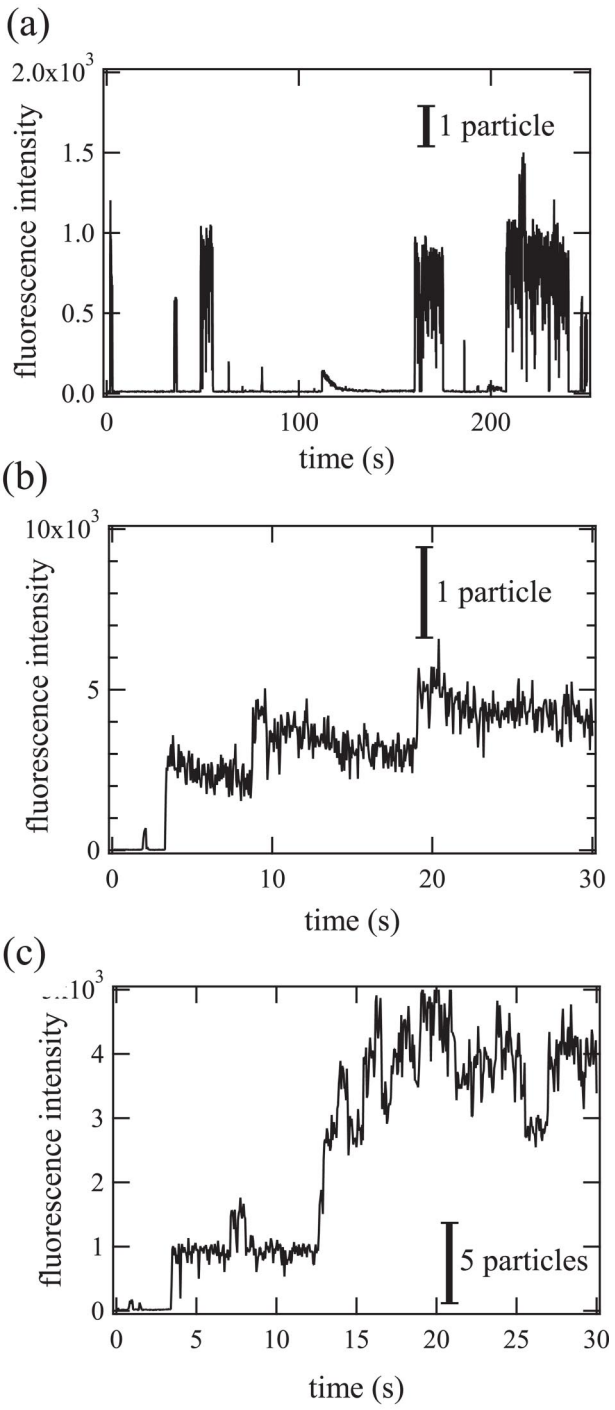

FIG. 4. Temporal trapping profiles of 40-nm-sized particles in water at the concentration of (a),(b) 8.8×10^7 and (c) 1.8×10^9 particles/ml. The laser power is (a),(c) 300 and (b) 900 mW. Vertical bars indicate fluorescence intensity corresponding to the particle number described beside each bar.

assembled one by one, agree with the experimental results. Figures 5(a) and 5(b) exemplify the temporal profiles of 40-nm-sized particle suspensions in the simulation at laser powers of 300 and 900 mW, respectively. We used the Derjaguin-Landau-Verwey-Overbeek (DLVO) potential with the repulsive barrier of $\sim 2kT$, as shown in Fig. 5(c). At the laser power of 300 mW, even if a single particle is trapped, it escapes immediately from the focal spot. Therefore the nanoparticles escaped from the optical trapping drift around the focal point. The increase of local concentration makes the clustering frequency increase. Clusters once formed stay at the focal spot for a longer time than the individual nanoparticles, which gives the characteristic temporal profiles, where clusters of 2–3 particles are frequently found. These results of the MC simulation indicate that our proposed model gives a consistent explanation of the optical assembling process of nanoparticles.

IV. CONCLUSIONS

As a first step to reveal the optical assembling process of nanoparticles, we have investigated the assembling dynamics of a single nanoparticle under the optical gradient force. The assembling process of nanoparticles was clarified by time evolution of the fluorescence intensity of nanoparticles. In the case of the strong trapping potential ($U_{\mathrm{trap}} \gg kT$), e.g., 100-nm-sized particles at the laser power of 300 mW or 40-nm-sized particles at 900 mW, it was observed that nanoparticles were assembling one by one at the focal spot. This process was explained as a diffusion-limited assembling process.

In contrast, in the case of a weak trapping potential ($U_{\mathrm{trap}} \sim kT$), e.g., 40-nm-sized particles at 300 mW, it was observed that a few particles were simultaneously trapped and then escaped from the focal spot. Furthermore, the results of the simple numerical simulation suggested that the clustering was induced by increase of the local particle density and then the cluster was likely trapped since the formed cluster had a large polarizability. It is expected that the characteristic assembling process, which is attributed to the weak interparticle potential, would be observed in a protein crystal. Protein crystal growth shows some states of assembling during nucleation and the clusters affect whether crystals are finally obtained. Our study indicates that optical assembly could control such states of clustering. Optical assembly mediated by clustering in the micrometer-sized region has the possibility to produce an assembly that cannot be obtained by conventional perturbations, i.e., stirring, evaporation, and addition of salt.

ACKNOWLEDGMENTS

The present work was partly supported by a Grant-in-Aid for Scientific Research (KAKENHI) (S) (14103006) from the Japan Society for the Promotion of Science (JSPS) and a Grant-in-Aid for Young Scientists (B) (14740384) to H.Y. from the Ministry of Education, Culture, Sports, Science and Technology of Japan. C.H. is supported by JSPS.

APPENDIX: SIMULATION PROTOCOL

The MC simulation is performed in a 2D system, where nanoparticles are dispersed and moved. The center of the focused laser beam is set at the origin of coordinates and a particle positioned at $\mathbf{r}=(x,y)$ is attracted toward the focal

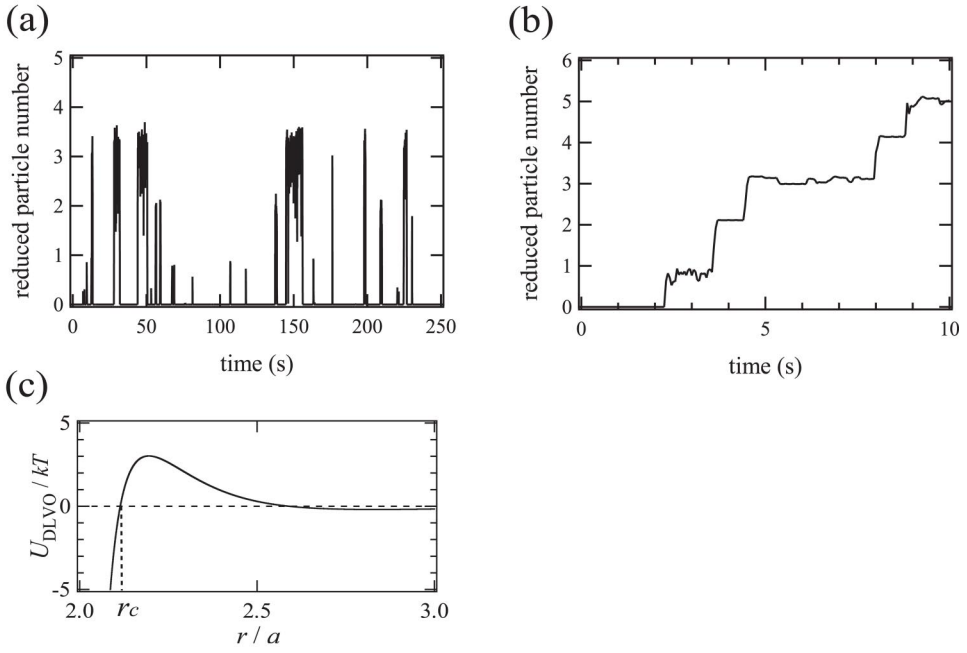

FIG. 5. Numerical simulation of assembling processes of 40-nm-sized particles. Simulations are performed at the same concentration of 14 particles/$(30\times30\ \mu m^2)$ and the laser power is (a) 300 and (b) 900 mW. (c) DLVO pair potential including attractive and repulsive potentials [31]. The potential energy U_{DLVO} in units of kT is plotted against the center-to-center distance r in units of the particle radius a of 40 nm. Debye length $1/\kappa$ is 3.04 nm. In the case of the distance $r_c<2.1a$, particles are regarded as a cluster.

point due to the optical gradient force. This potential energy U_{trap} is expressed as

$$U_{trap}(r) \cong -\alpha|\mathbf{E}|^2/2, \quad \text{(A1)}$$

where $\mathbf{E}$ is the electric field. α is the polarizability of the particle under the dipole approximation and is given by $\alpha=4\pi\varepsilon_2 a^3[(n_1/n_2)^2-1]/[(n_1/n_2)^2+2]$, where a is the radius of the particle, n_1 and n_2 are the refractive indices of the particle and the surrounding medium, respectively, and ε_2 is the dielectric constant of the medium. The beam intensity I is described as

$$I(\mathbf{r}) = (\varepsilon_2 c/2n_2)|\mathbf{E}|^2 = (2P/\pi w_0^2)\exp(-2\mathbf{r}^2/w_0^2), \quad \text{(A2)}$$

in which w_0 is the beam waist, and P is the beam power. The three-dimensional fluorescence intensity distribution was measured and confirmed to be reproduced by a Gaussian function, from which its parameters were determined.

The Derjaguin-Landau-Verwey-Overbeek potential [31] U_{DLVO} is represented by the combination of attractive and repulsive potentials: $U_{DLVO}=U_{att}(r)+U_{rep}(r)$. $U_{att}(r)$ is the van der Waals attractive potential and $U_{rep}(r)$ is the electrostatic Coulomb repulsive potential. The parameter values to determine the DLVO potential are set as follows: the radius of the particle $a=20$ nm, the absolute temperature $T=298$ K, and the effective Hamaker constant $A_H=1$ eV. The particle surface potential $\psi_0=-44.0$ mV is determined from the zeta potential. The Debye length $1/\kappa$ is calculated as 3.04 nm from these parameters. The DLVO potential used in the simulation is shown in Fig. 5(c).

The simulation protocol is based on a standard Metropolis Monte Carlo simulation [32,33]. All simulations are executed in a $30\times30\ \mu m^2$ sized two-dimensional simulation cell with periodic boundary conditions. At the start of the simulation, particles are randomly positioned. In each Monte Carlo step, we generated a random step whose maximum length $r_{max}=3a$. In one step, each particle is moved to the next destination where the total potential energy $(U_{trap}+U_{DLVO})$ is smaller than that of the previous position. The time interval Δt at each step is assigned as $\Delta t=\langle r_{max}^2\rangle/2D\sim165\ \mu s$, where D is a diffusion coefficient obtained by DLS measurement of 40-nm-sized particles. The positions of particles are recorded at each 0.05 s, which corresponds to the experimental conditions.

As a model of clustering particles, we included a cluster-moving process in our MC simulation. In the simulation process, adjacent particles within the distance $r_c=2.1a$ are treated as a cluster whose volume is N times as large as a single particle, where N is the particle number in the cluster. To obtain the temporal profiles of the two-photon fluorescence intensity of trapped particles, we calculated the sum of squares of the laser intensity irradiated on each trapped particle located at $\mathbf{r}_i$ ($|\mathbf{r}_i|<2\ \mu m$), that is, $\Sigma_i I^2(\mathbf{r}_i)$.

[1] A. Ashkin, M. J. Dziedzic, E. J. Bjorkholm, and S. Chu, Opt. Lett. **11**, 288 (1986).
[2] A. Ashkin, IEEE J. Sel. Top. Quantum Electron. **6**, 841 (2000).
[3] K. Sasaki, M. Koshioka, H. Misawa, N. Kitamura, and H. Masuhara, Jpn. J. Appl. Phys., Part 2 **30**, L907 (1991).
[4] K. Sasaki, M. Koshioka, H. Misawa, N. Kitamura, and H. Masuhara, Appl. Phys. Lett. **60**, 807 (1992).
[5] D. G. Grier, Nature (London) **424**, 810 (2003).
[6] S. Juodkazis, N. Mukai, R. Wakaki, A. Yamaguchi, S. Matsuo,

and H. Misawa, Nature (London) **408**, 178 (2000).
[7] A. Ehrlicher, T. Betz, B. Stuhrmann, D. Koch, V. Milner, M. G. Raizen, and J. Käs, Proc. Natl. Acad. Sci. U.S.A. **99**, 16024 (2002).
[8] M. Ichikawa, Y. Matsuzawa, Y. Koyama, and K. Yoshikawa, Langmuir **19**, 5444 (2003).
[9] S. Ito, H. Yoshikawa, and H. Masuhara, Appl. Phys. Lett. **80**, 482 (2002).
[10] M. M. Burns, J.-M. Fournier, and J. A. Golovchenko, Phys. Rev. Lett. **63**, 1233 (1989).
[11] M. M. Burns, J.-M. Fournier, and J. A. Golovchenko, Science **249**, 749 (1990).
[12] D. Mei, B. Cheng, W. Hu, Z. Li, and D. Zhang, Opt. Lett. **20**, 429 (1995).
[13] S. A. Tatarkova, A. E. Carruthers, and K. Dholakia, Phys. Rev. Lett. **89**, 283901 (2002).
[14] D. McGloin, A. E. Carruthers, K. Dholakia, and E. M. Wright, Phys. Rev. E **69**, 021403 (2004).
[15] J. Hofkens, J. Hotta, K. Sasaki, and H. Masuhara, J. Am. Chem. Soc. **119**, 2741 (1997).
[16] J. Hotta, K. Sasaki, and H. Masuhara, J. Am. Chem. Soc. **118**, 11968 (1996).
[17] P. Borowicz, J. Hotta, K. Sasaki, and H. Masuhara, J. Phys. Chem. B **101**, 5900 (1997).
[18] S. Masuo, H. Yoshikawa, T. Asahi, H. Masuhara, T. Sato, D-L. Jiang, and T. Aida, J. Phys. Chem. B **106**, 905 (2002).
[19] U. Gasser, E. R. Weeks, A. Schofield, P. N. Pusey, and D. A. Weitz, Science **292**, 258 (2001).
[20] A. Yethiraj and A. van Blaaderen, Nature (London) **421**, 513 (2003).
[21] A. Pertsinidis and X. S. Ling, Nature (London) **413**, 147 (2001).
[22] W. J. Soppe and G. J. M. Janssen, J. Chem. Phys. **96**, 6996 (1992).
[23] N. Olivi-Tran, R. Botet, and B. Cabane, Phys. Rev. E **57**, 1997 (1998).
[24] E. L. Florin, J. K. H. Horber, and E. H. K. Stelzer, Appl. Phys. Lett. **69**, 446 (1996).
[25] N. G. van Kampen, *Stochastic Processes in Physics and Chemistry* (North-Holland, Amsterdam, 1992), Chap. 8.
[26] L. E. Helseth, T. M. Fischer, and T. H. Johansen, Phys. Rev. E **67**, 042401 (2003).
[27] L. E. Helseth, H. Z. Wen, T. M. Fischer, and T. H. Johansen, Phys. Rev. E **68**, 011402 (2003).
[28] L. E. Helseth and T. M. Fischer, Opt. Express **12**, 3428 (2004).
[29] J. N. Israelachvili, *Intermolecular and Surface Forces* (Academic, New York, 1992)
[30] K. Svoboda and S. M. Block, Opt. Lett. **19**, 930 (1994).
[31] E. J. W. Verwey and J. Th. G. Overbeek, *Theory of the Stability of Lyphobic Colloids* (Elsevier, Amsterdam, 1948).
[32] N. Metropolis, A. W. Rosenbluth, and E. Teller, J. Chem. Phys. **21**, 1087 (1953).
[33] M. P. Allen and D. J. Tildesley, *Computer Simulation of Liquids* (Clarendon, Oxford, 1987), Chap. 4.